In Situ Monitoring of Atomic Layer Controlled Pore Reduction in Alumina Tubular Membranes Using Sequential Surface Reactions

B. S. Berland,† I. P. Gartland, A. W. Ott,‡ and S. M. George*

Department of Chemistry and Biochemistry, University of Colorado, Boulder, Colorado 80309

Received May 28, 1998. Revised Manuscript Received July 24, 1998

The pore diameter in alumina tubular membranes with an initial diameter of 50 Å was systematically reduced using the atomic layer controlled deposition of Al_2O_3. The Al_2O_3 was deposited using sequential exposures of $Al(CH_3)_3$ (trimethylaluminum, TMA) and H_2O in an ABAB... binary reaction sequence. The pore diameter reduction was monitored using in situ N_2 and Ar conductance measurements. The conductance, $C = Q/\Delta P$, was measured using a mass flow controller to define a constant gas throughput, Q, and a pair of capacitance manometers to monitor the transmembrane pressure drop, ΔP. Conductance measurements were periodically obtained at 298 K as a function of AB binary reaction cycles. These conductance measurements were consistent with a pore diameter reduction from 50 Å to ∼5−10 Å at a rate of ∼2.5 Å for each AB cycle. Conductance measurements were also performed during the Al_2O_3 deposition at 500 K after each half-reaction in the binary reaction sequence. The TMA half-reaction leaves the pore surface covered with $AlCH_3$* surface species; the H_2O half-reaction converts these surface species to AlOH*. Following the TMA exposures, the conductance was significantly lower than the conductance after the subsequent H_2O exposure. The corresponding difference in pore diameter of $\Delta D \approx 2$ Å was close to the difference predicted by the van der Waals hard sphere diameters of 3.5−4.0 Å for a CH_3 group and 2.9 Å for an OH group. These in situ conductance measurements demonstrate that the pore diameters in mesoporous membranes can be reduced to molecular dimensions with atomic layer control using sequential surface reactions. Pore diameters can be tailored for specific applications by varying the number of AB cycles and changing the nature of the terminating surface functional groups.

I. Introduction

Porous inorganic membranes have a wide variety of applications because of their high mechanical, chemical, and thermal stability.[1] These characteristics make porous inorganic membranes especially appealing for gas separation membranes. However, most available inorganic membranes are limited to mesoporous structures with diameters of ∼40−50 Å, where transport through the pores is governed by Knudsen diffusion. In the Knudsen regime, the selectivity of the membranes is dictated only by the molecular masses, and large gas separation factors are not possible. The separation properties of these membranes can be dramatically improved by reducing the pore size to molecular diameters where surface interactions and molecular sieving effects become increasingly important.

Several groups have developed chemical vapor deposition (CVD) methods to modify inorganic membranes to improve selectivities.[2−9] Many of these studies employed CVD of SiO_2 films in Vycor glass or alumina tubes to reduce the pore sizes.[2−5,7,9] CVD can be used effectively to close off pores and achieve high separation ratios for small gases, such as H_2 and He, relative to larger gases. However, CVD techniques do not have a large degree of control over the final pore size or thickness of the deposited layer. Thick separation layers are often observed with poor permeabilities. The lack of controlled growth also prevents the tailoring of pore sizes for the separation of molecules larger than H_2 and He.

Controlled pore reduction and thickness control is easily attained using atomic layer controlled deposition techniques.[8,10,11] Two component films can be deposited by sequential exposures of the appropriate precursors

† Current Address: ITN Energy Systems, Wheat Ridge, CO 80033.
‡ Current Address: Department of Materials Sci. and Engineering, Northwestern University, Evanston, IL 60208.

(1) Bhave, R. R. *Inorganic Membranes: Synthesis, Characteristics and Applications*; Van Nostrand Reinhold: New York, 1991.
(2) Ha, H. Y.; Nam, S. W.; Hong, S. A.; Lee, W. K. *J. Membr. Sci.* **1993**, 85, 279.
(3) Wu, J. C. S.; Sabol, H.; Smith, G. W.; Flowers, D. L.; Liu, P. K. T. *J. Membr. Sci.* **1994**, *96*, 275.
(4) Tsapatsis, M.; Gavalas, G. *J. Membr. Sci.* **1994**, *87*, 281.
(5) Onuki, K.; Nakajima, H.; Shimuzu, S.; Nagoshi, M. *J. Chem. Eng. Jpn.* **1997**, *30*, 359.
(6) Xomeritakis, G.; Han, J.; Lin, Y. S. *J. Membr. Sci.* **1997**, 124, 27.
(7) Kim, S.; Gavalas, G. R. *Ind. Eng. Chem. Res.* **1995**, *34*, 168.
(8) Ott, A. W.; Klaus, J. W.; Johnson, J. M.; George, S. M.; McCarley, K. C.; Way, J. D. *Chem. Mater.* **1997**, *9*, 707.
(9) Sea, B.-K.; Kusakabe, K.; Morooka, S. *J. Membr. Sci.* **1997**, *130*, 41.
(10) George, S. M.; Ott, A. W.; Klaus, J. W. *J. Phys. Chem.* **1996**, *100*, 13121.
(11) Ott, A. W.; McCarley, K. C.; Klaus, J. W.; Way, J. D.; George, S. M. *Appl. Surf. Sci.* **1996**, *107*, 128.

10.1021/cm980384g CCC: $15.00
Published on Web 11/04/1998

in an ABAB... binary reaction scheme.[10,12,13] For Al_2O_3 deposition, the binary reaction $2Al(CH_3)_3 + 3H_2O \rightarrow Al_2O_3 + 6CH_4$ is split into two half-reactions:[8,10,11,14−16]

$$AlOH^* + Al(CH_3)_3 \rightarrow AlOAl(CH_3)_2^* + CH_4 \quad (A)$$

$$AlCH_3^* + H_2O \rightarrow AlOH^* + CH_4 \quad (B)$$

where the asterisk designates the surface species. These A and B half-reactions are self-terminating at coverages near one monolayer. This self-limiting chemistry allows for conformal deposition in high aspect ratio structures such as mesoporous and microporous membranes with atomic layer control of the deposited layer thickness.

Previous studies have successfully employed atomic layer controlled deposition of Al_2O_3 to reduce the pore size of mesoporous Anodisc alumina membranes.[8] The Al_2O_3 layers were deposited using sequential exposures of $Al(CH_3)_3$ (trimethylaluminum, TMA) and H_2O and the pore diameters were reduced from 200 to 140 Å. However, these studies required ex situ monitoring of the pore diameter, and exposure of the modified membranes to air led to fouling for the smaller pore diameters. Consequently, pore reduction was not verifiable for diameters <140 Å.[8] Similar techniques have been used to develop H_2 permselective membranes by depositing SiO_2 in Vycor tubes.[7]

In the current study, a new deposition flow reactor has been constructed for efficient atomic layer controlled deposition on porous membranes, flat substrates, or particles. This new deposition chamber was employed to modify asymmetric alumina tubular membranes with a nominal starting pore diameter of 50 Å. TMA and H_2O exposures were performed in an alternating binary reaction sequence to reduce systematically the pore size to molecular dimensions. The deposition flow reactor was designed for in situ monitoring of the pore diameter using N_2 and Ar conductance measurements. The conductance measurements observed the progressive reduction of the pore diameter versus the TMA and H_2O reaction cycles and distinguished conductance differences for CH_3 and OH groups on the pore surface.

II. Experimental Section

A. Deposition Chamber and Gas Manifold. The new deposition chamber used for the pore reduction experiments is shown in Figure 1. The high vacuum chamber was pumped by a 600 L/s diffusion pump that could be isolated from the chamber with a gate valve. For high-pressure experiments, the chamber was pumped with a dual stage mechanical pump. The chamber pressure could be monitored with either a nude ionization gauge or a 1000 Torr Baratron absolute pressure gauge. The chamber was also equipped with a Dycor mass spectrometer for residual gas analysis.

The $Al(CH_3)_3$ (trimethylaluminum, TMA, Aldrich 97%) and H_2O (distilled and deionized) reactant gases were introduced into the membrane pores via the gas manifold shown in Figure 2. Trimethylaluminum (TMA) is a pyrophoric liquid. The TMA was transferred to a stainless steel reservoir equipped with Nupro valves using a glovebag filled with N_2. The stainless steel reservoirs of liquid TMA or H_2O were purified with several freeze−pump−thaw cycles using liquid nitrogen. The TMA and H_2O vapors above these reservoirs could be transported to the alumina tubular membranes either directly or by entrainment in a N_2 carrier gas stream.

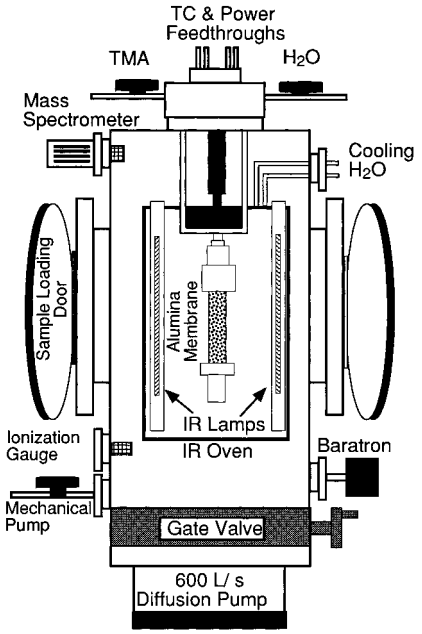

Figure 1. Schematic representation of the deposition chamber used for the pore reduction experiments.

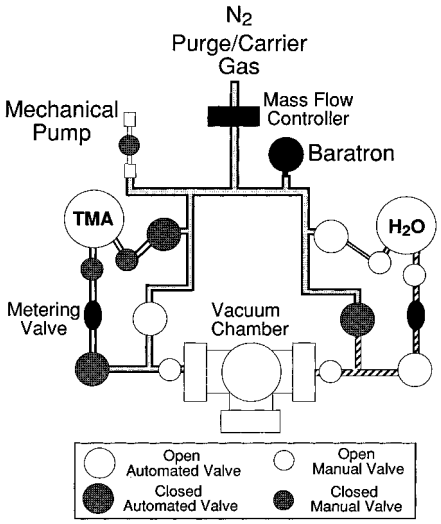

Figure 2. Representation of the gas manifold showing the valve settings during a H_2O exposure and N_2 purge of the TMA side of the gas line.

Al_2O_3 was deposited in the pores using sequential half-reactions with TMA and H_2O. One AB cycle consisted of a TMA exposure/N_2 purge/H_2O exposure/N_2 purge. The manifold could easily be switched between reactant exposure and purge modes using automated on−off valves from General Valve, as illustrated in Figure 2. The gas manifold was also connected to a dual stage mechanical pump. The N_2 purge or carrier gas flow was controlled using a 1−100 sccm mass flow controller. Metering valves after the TMA and H_2O reservoirs could also be employed to control the partial pressure of reactants exposed to the alumina tubular membranes.

Figure 3 displays a typical dosing sequence for Al_2O_3 deposition when the reactant gases are entrained in a N_2 carrier gas. Figure 3a shows the H_2O (m/e = 18) mass spectrometer signal after the gas manifold is switched to the H_2O exposure mode shown in Figure 2. The ~30 s time delay is consistent with the transport time for H_2O to move the length of the gas line and permeate the alumina membrane. The H_2O mass spectrometer signal decreases to the original

(12) Suntola, T.; H. J. *Annu. Rev. Mater. Sci.* **1985**, *15*, 177.
(13) Goodman, C. H.; Pessa, M. V. *J. Appl. Phys.* **1986**, *60*, R65.

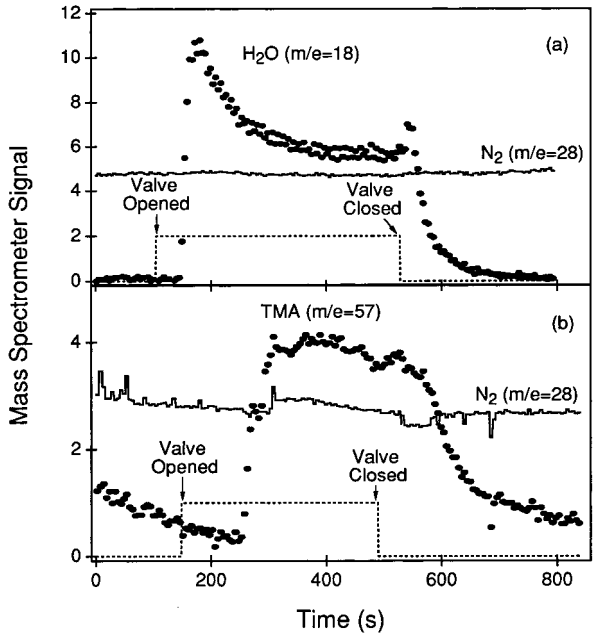

Figure 3. Exposure sequence for reactant gases entrained in a N_2 carrier gas: (a) mass spectrometer signals for H_2O (circles) and N_2 (solid line) during a H_2O exposure and (b) mass spectrometer signals for TMA (circles) and N_2 (solid line) during a TMA exposure.

level shortly after the manifold is switched back to the N_2 purge mode with a delay time consistent with gas transport times. The N_2 ($m/e = 28$) mass spectrometer signal remains constant throughout the H_2O exposure.

The H_2O initial spike in Figure 3a is attributed to a build up of H_2O vapor between the H_2O reservoir and the automated valve prior to the opening of the automated valve. The H_2O flow is conductance-limited by the metering valve. With the automated valve closed, the H_2O pressure equilibrates on both sides of the metering valve. This leads to the initial H_2O pressure spike shown in Figure 3a. After this transient, the conductance-limiting metering valve produces H_2O pressure at the inlet of the automated valve that is less than the 20 Torr H_2O vapor pressure at room temperature.

Similar results are observed during the TMA exposure, as shown in Figure 3b. The mass spectrometer signal for the main mass spectrometer cracking fragment of TMA ($m/e = 57$) increases shortly after the manifold is switched to the TMA exposure mode. This TMA signal decreases shortly after the valves are returned to the N_2 purge mode. The delay times for TMA are somewhat longer than those for H_2O because the TMA conductance through the pores is slightly smaller. TMA is expected to have a smaller conductance based on mass difference and Knudsen diffusion through the porous membrane.

During the deposition of Al_2O_3 in the pores, the conductance of the membrane progressively decreased versus AB cycles. As a result, the metering valve settings had to be continuously adjusted to maintain constant reactant exposures. An exposure scheme with the reactants entrained in a N_2 carrier gas as illustrated in Figure 3 is ideal for deposition on flat substrates when the conductance remains constant. For the changing conductance in mesoporous or microporous membranes, reactant exposures are defined more easily using the reactant vapor pressure with no N_2 carrier gas. This exposure method was utilized for the Al_2O_3 deposition and the Baratron was employed to measure the reactant exposures.

B. Infrared Oven for Membrane Heating. The rapid thermal annealing infrared (IR) oven used to heat the alumina membranes is shown schematically in Figure 1. The oven consists of four ~9 in. IR lamps housed in a stainless steel reflector. The IR lamps were evenly distributed around the membrane for uniform heating. The temperature of the oven could be controlled by varying the voltage supplied to the lamps. A broad range of temperatures from 300 to 1000 K could be achieved with this heating scheme. Type K chromel−alumel thermocouple wires were attached to the alumina membrane and the stainless steel oven housing to monitor the temperature. The IR oven also encased the last portion of the reactant gas supply line. This design preheats the reactant gases to the reaction temperatures prior to exposure to the membranes.

Rapid thermal heating of the alumina tubular membranes could easily be attained with this setup. However, the radiative cooling of the IR oven was inefficient, and the cooling times of the samples were excessively long. To decrease the cooling times, H_2O cooling lines were added to provide a thermal cooling reservoir. With H_2O cooling, the membrane could still only be cooled from 500 to 300 K in ~4 h.

C. Membrane Mounting and Cleaning. Asymmetric γ-alumina tubular membranes from U.S. Filter Ceramic Membrane Products (Warrendale, PA) were used for these studies. The tubes were ~50 mm long with an inner diameter of ~7 mm and an outer diameter of ~10 mm. The support layers consisted of a 0.8 μm pore diameter layer that was 40 μm thick and a 0.2 μm pore diameter sol−gel layer that was 20 μm thick coated on the inner wall of a 10−12 μm extruded support.[17] The final limiting layer was a 3−5 μm thick sol−gel layer with an average pore diameter of 50 Å.[17] Mercury intrusion and gas permeability methods have been used to characterize the pore diameters and 90% of all the pore diameters are between 45 and 55 Å.[17] The ends of the tubular membranes were sealed with a commercial ceramic glaze to ensure gas flow through the smallest pore diameters. The membrane was interfaced with the reactant gas lines using stainless steel Swagelok fittings and graphite ferrules. The other end of the membrane was plugged with a Swagelok cap to force the gas flow through the pores in the tubular membrane walls.

Past studies have shown that small diameter pores readily adsorb organic molecules and H_2O in air over time.[8,18] Prior to Al_2O_3 deposition, the pores could be cleared by treatment with 30% H_2O_2 or HNO_3, in agreement with previous observations.[8] However, additional fouling was observed after the cleaned membranes were mounted in the vacuum chamber. This pore clogging was attributed to outgassing of organics and H_2O from the chamber walls. To clean the membranes in situ, the membranes were heated to 800 K in the IR oven to remove any adsorbed molecules from the pores.[14] This heating also removed organics and H_2O from the chamber walls and eliminated subsequent fouling problems.

D. Al_2O_3 Deposition. Al_2O_3 was deposited in the pores using the ABAB... binary reaction sequence defined previously. To attain atomic layer controlled deposition of Al_2O_3 using the binary reaction sequence, the A and B reactant exposures must be sufficiently separated to avoid overlap that would lead to conventional chemical vapor deposition (CVD). In addition, each reaction should be performed to completion to obtain the most efficient growth. Previous experiments have reported that reactant exposures of $P \sim 0.5$ Torr for ~2 min at 500 K are sufficient for saturation in alumina membranes with pore diameters of ~2000 Å.[8,11]

Because of possible conductance limitations in small pore diameters, larger reactant exposures were used to demonstrate that the atomic layer controlled growth techniques could be extended to deposition in pores with diameters ≤ 50 Å. The following sequence of exposures constituted one AB cycle at 500 K. First, the pores in the tubular alumina membrane were

(14) Dillon, A. C.; Ott, A. W.; Way, J. D.; George, S. M. *Surf. Sci.* **1995**, *322*, 230.
(15) Soto, C.; Tysoe, W. T. *J. Vacuum Sci. Technol. A* **1991**, *9*, 2686.
(16) Higashi, G. S.; Flemming, C. G. *Appl. Phys. Lett.* **1989**, 55, 1963.
(17) Bhave, R. R.; Filter, U. S. Personal communication, 1997.
(18) Funke, H. H.; Frender, K. R.; Green, K. M.; Wilwerding, J. L.; Sweitzer, B. A.; Falconer, J. L.; Noble, R. D. *J. Membr. Sci.* **1997**, *129*, 77.

subjected to a 10 min, 2 Torr H_2O exposure. The mass spectrometer showed H_2O appearing in the chamber within 30 s of opening the H_2O reservoir. The H_2O peak at $m/e = 18$ also decreased rapidly after closing the H_2O reservoir. Excess H_2O reactant was then removed from the gas lines by pumping with the mechanical pump for 15 min. Subsequently, the gas lines were purged with N_2 for 30 min at a N_2 flow rate of 1 sccm.

Following H_2O removal and purging, the pores were subjected to a 15 min, 2 Torr TMA exposure. The mass spectrometer showed cracking patterns consistent with TMA within 30 s of initiating the TMA exposure. At short TMA exposure times, the CH_4 peak at $m/e = 15$ was the largest peak in the mass spectrum. A small $Al(CH)_2$ signal at $m/e = 57$ also appeared that is the main cracking fragment of TMA.[19] The TMA exposure time of 15 min was chosen because this was the time required for the TMA mass spectrometric peak at $m/e = 57$ to become larger than the CH_4 peak.

The large increase in the TMA peak intensity that was concurrent with the decrease in the CH_4 peak intensity suggested that the TMA half-reaction had reacted to completion. The remaining CH_4 mass spectrum signal was attributed to TMA reaction with OH groups or H_2O on the chamber walls. Unfortunately, the TMA exposures were detrimental to the mass spectrometer and the use of the mass spectrometer to follow the progress of the reaction was not possible after these initial measurements. The TMA exposure was followed by 15 min of pumping using the mechanical pump and a N_2 purge for 30 min at a N_2 flow rate of 1 sccm.

These long reactant exposures are most likely excessive and should be sufficient for the surface reactions to reach completion, even in the smallest pore diameters with the lowest conductance. However, the AB cycle time of 2 h was prohibitively slow. Consequently, a series of tests were performed to determine the procedures that were necessary to obtain atomic layer controlled growth with the minimum cycle time. Pumping with the mechanical pump to remove excess reagents was eliminated without effecting the observed growth rates. The N_2 purge time was also systematically reduced from 45 to 10 min without increasing the Al_2O_3 growth rate.

Slightly increased growth rates were observed with N_2 purge times of ≤ 5 min that were consistent with some conventional chemical vapor deposition. Purge times shorter than 5 min may be possible with larger N_2 flow rates. Similar growth rates were also observed when H_2O and TMA reactant exposures were reduced from 15 to 5 min. The resulting AB cycle for atomic layer controlled growth of Al_2O_3 at 500 K with minimum cycle time was (1) dose H_2O at 10 Torr for 5 min; (2) purge with N_2 at 1 sccm for 10 min; (3) dose TMA at 10 Torr for 5 min; and (4) purge with N_2 at 1 sccm for 10 min.

E. Conductance Measurements. The pore diameter reduction was monitored using in situ N_2 conductance measurements at 298 K. For these measurements, the N_2 flow, Q, was set with the 1−100 sccm mass flow controller and the system was allowed to reach equilibrium. At equilibrium, the flow through the porous membrane is equal to the flow through the mass flow controller. For each flow rate, the transmembrane pressure, ΔP, was monitored using the two 1000 Torr Baratron absolute pressure transducers, one on the feed (manifold) side and one on the downstream (chamber) side. The conductance, C, is then calculated using $C = Q/\Delta P$. The conductance was measured for a series of flows from either Q = 1−100 sccm or ΔP = 1−1000 Torr, depending on the conductance of the membrane.

Gas transport through the 50 Å pores of the initial unmodified mesoporous membrane should be defined by Knudsen flow. Knudsen flow occurs when the Knudsen number, $K_n = \lambda/r \gg 1$, where λ is the mean free path of the permeating gas and r is the pore radius. For N_2 flow through the 50 Å diameter pores, $K_n = 10-10^4$ at pressures of 1000−1 Torr. Under these conditions, the N_2 transport through the pores should be in Knudsen flow and the conductance through the pores, C_p, should be independent of the pressure.

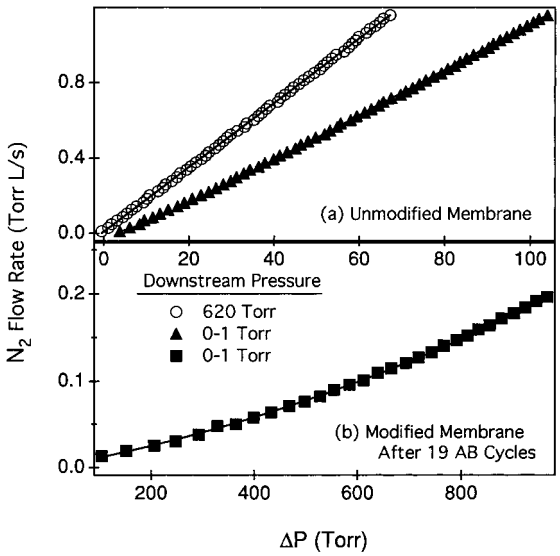

Figure 4. N_2 conductance measurements of (a) unmodified mesoporous alumina tubular membrane and (b) the modified membrane after 19 AB cycles. Measurements were conducted with the downstream pressure at 620 Torr (open symbols) and 0−1 Torr (solid symbols).

However, Figure 4a clearly shows the conductance is pressure-dependent. Different conductances were measured depending on whether the downstream pressure was at atmosphere (620 Torr) or vacuum (0−1 Torr). These pressure-dependent conductance measurements suggest a small viscous flow component to the N_2 transport because viscous flow transport is directly proportional to pressure. The viscous flow component is consistent with defects in the membrane structure, sealing difficulties or conductance limitations caused by transport through the gas line.

The pressure-dependent conductance measurements could be caused by defects or cracks in the 50 Å porous layer of the tubular membrane. Large cracks or defects in the 50 Å porous layer would directly expose the gas flow to the Al_2O_3 support layer with 2000 Å pores. These ∼2000 Å pores have a Knudsen number of $K_n \sim 1-10^3$ over the pressure range of the measurements. Purely Knudsen flow may not occur until $K_n > 100$.[20] Mixed Knudsen and viscous flow have been reported in the literature for membranes with pore sizes on the order of 1000 Å and transmembrane pressures of ∼760 Torr.[1,21,22]

Pinholes in the ceramic glaze on the sealing ends of the tubular membranes or difficulties with the Swagelok sealing would also lead to viscous flow contributions. Improvements in the initial selectivities of the U.S. Filter membranes were observed with several reglazed membranes. In addition, the glazed surface of the tubular membranes is not uniform. The slightly oblong shape of the glazed surface may be difficult to seal adequately with Swagelok connections designed for circular tubes. The viscous flow contribution from the defects or sealing will be designated as C_s and is in parallel with the conductance of the pores.

Transport of gases through the $^1/_8$ in. gas lines is in viscous flow ($K_n < 0.01$) over the entire range of pressures employed in these studies. To account for this viscous flow, the conductance of the gas lines, C_g, was measured independently without a tubular membrane mounted in the vacuum chamber. This pressure-dependent conductance was measured to be C_g

(19) Tanaka, J.; Smith, S. R. *Inorg. Chem.* **1969**, *8*, 265.

(20) Barrer, R. M. *Zeolites and Clay Materials as Sorbents of Molecular Sieves*; Academic Press: London, England, 1978.

(21) Keizer, K.; Ulhorn, R. J. R.; van Vuren, R. J.; Burggraaf, A. J. *J. Membr. Sci.* **1988**, *39*, 285.

(22) Schofield, R. W.; Fane, A. G.; Fell, C. J. D. *J. Membr. Sci.* **1990**, *53*, 159.

$= 0.0016P$(Torr) L/s. C_g alone in series with C_p could not explain the pressure-dependent data shown in Figure 4a.

The total measured conductance is a sum of all the contributions from C_p, C_s, and C_g. Conductances in parallel add and conductances in series add as reciprocals. Consequently, the total conductance is described by

$$C_T = C_g(C_s + C_p)/(C_s + C_p + C_g) \quad (1)$$

By using the measured value of the gas line conductance, C_g, the measurements of ΔP versus Q can be fit to obtain C_p and C_s.

The gas flux through the alumina membrane is in Knudsen flow for pore diameters 20 Å $< D <$ 500 Å in the mesoporous region. For Knudsen flow, the measurement of C_p can then be used to determine the pore diameter, D. If the pores are assumed to be cylindrical, the conductance is $C \propto D^3$. C_p can then be used to obtain the pore diameter using the initial conductance through the pores, C_o, and assuming an initial pore diameter of $D_o = 50$ Å:

$$D = D_o(C_p/C_o)^{1/3} \quad (2)$$

The conductance through the 50 Å porous layer may also be limited by the narrow gaps between the Al_2O_3 particles rather than the connecting channels. If the pores behave like apertures, the conductance is $C \propto D^2$. C_p can then be used to obtain the pore diameter using

$$D = D_o(C_p/C_o)^{1/2} \quad (3)$$

The true conductance may be a combination of cylinders and apertures with a pore diameter dependence intermediate between D^2 and D^3.

The gas diameter becomes comparable to the pore diameter in the microporous region for pore diameters $D <$ 20 Å. In this regime, a transition can occur from Knudsen diffusion to configurational diffusion.[23,24] This transition is dependent on the gas diameter, gas−surface interactions, and the pore diameter.[23] For small, relatively inert molecules such as N_2 and Ar, this transition is not expected to occur until pore diameters of 5−10 Å.[23] Consequently, the C_p measurements will be utilized to estimate pore diameters $D <$ 20 Å assuming Knudsen flow.

III. Results and Discussion

A. Conductance Measurements. Figure 4a shows typical conductance measurements for the initial mesoporous alumina tubular membrane at 298 K. Although the solid triangles and open circles can be fit with straight lines that are consistent with pure Knudsen flow, the different conductances measured with the downstream pressure at vacuum and atmosphere show a pressure-dependent conductance. The solid lines show the fit to Figure 4a using eq 1. The best fit was obtained with $C_p = 0.013$ L/s and $C_s = 1 \times 10^{-7}P$(Torr) L/s. As expected, these conductances indicate that transport through the initial unmodified tube is primarily determined by Knudsen flow. Almost all of the N_2 flow travels through the pores at low pressures. As much as 10% of the N_2 flow goes through the viscous flow leak at the highest pressures of 1000 Torr.

The fraction of the N_2 flow traveling through the pores decreases dramatically as the pore diameter is reduced with Al_2O_3 deposition. Figure 4b shows the conductance measurement for the same tube modified using 19 AB cycles with the original reaction conditions as described in the Experimental Section. This pore size reduction significantly reduces the membrane conductance as revealed by the larger ΔP and smaller Q values. The atomic layer growth reduces the pore diameter from 50 to 5−10 Å.

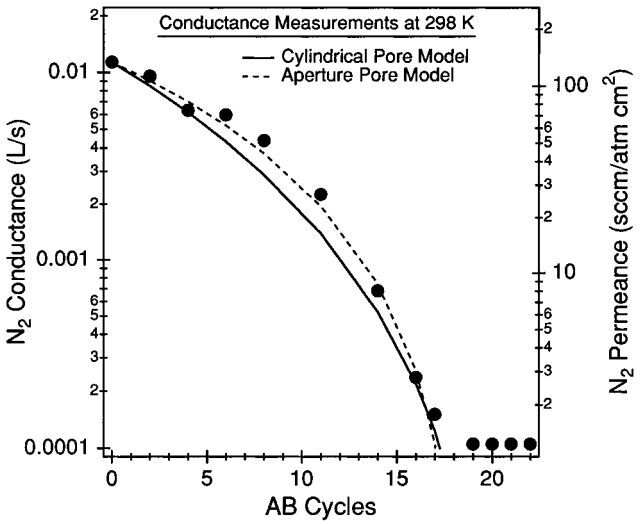

Figure 5. N_2 conductance and corresponding N_2 permeance at 298 K versus AB cycles. The solid and dashed lines represent the conductance changes predicted using the cylindrical pore and aperture pore models, respectively.

The ∼22 Å of Al_2O_3 deposited by the 19 AB cycles will have a minimal effect on the leaks through defects or cracks. Consequently, C_s is not expected to change with deposition. Because C_p and C_s are in parallel, their conductances add and the relative contribution of C_s to the total conductance increases during deposition. With increasing flow through the leaks, the conductance displays viscous flow behavior and becomes more pressure-dependent, as evidenced by the nonlinearity of the Q versus ΔP data in Figure 4b. The best fit to the data in Figure 4b is obtained with $C_p = 0.00011$ L/s and $C_s = 1 \times 10^{-7}P$(Torr) L/s. On the basis of this fit, as much as 50% of the N_2 flow travels through the leaks under viscous flow at the highest transmembrane pressures. Sufficient N_2 flow still goes through the pores to allow an accurate determination of C_p and the pore diameter with the N_2 conductance measurements.

B. Pore Reduction versus AB Cycles. The N_2 conductance through the pores, C_p, at 298 K as a function of AB cycles is displayed in Figure 5. The right-hand axis shows the area-normalized conductance, i.e., the permeance, using the unglazed tube length and the inner diameter of the tubular membrane to estimate the surface area. Figure 5 shows a dramatic decrease in conductance with Al_2O_3 deposition for the first 17−18 AB cycles. The decreased conductance is attributed to the decreasing pore diameter with Al_2O_3 deposition. These conductance changes were examined on several microporous alumina tubular membranes and were reproducible.

Assuming Knudsen flow, the change in the pore diameter can be obtained from the conductance measurements using eqs 2 and 3. Figure 6 shows the pore diameter as a function of AB cycles. The solid circles display the change in pore diameter using eq 2 and assuming the cylindrical pore model. The open squares

(23) Xiao, J.; Wei, J. *Chem. Eng. Sci.* **1992**, *47*, 1123.
(24) Shelekhin, A. B.; Dixon, A. G.; Ma, Y. H. *AIChE J.* **1995**, *41*, 58.

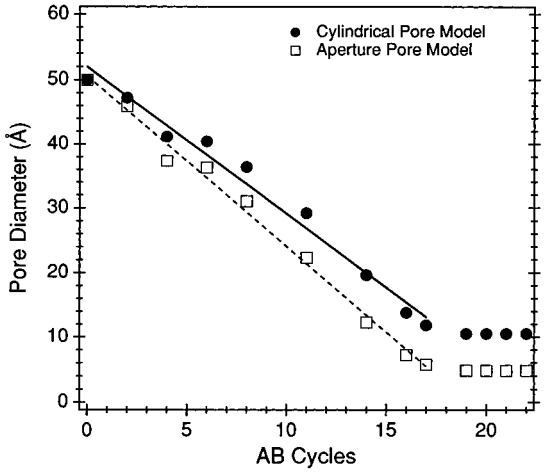

Figure 6. Pore diameter versus AB cycles. The pore diameters were calculated from the N_2 conductance versus AB cycles assuming Knudsen flow and using eqs 2 and 3 for the cylindrical pore (solid circles) and aperture pore models (open squares).

show the change in pore diameter using eq 3 and assuming the aperture model.

The solid line in Figure 6 is a linear least-squares fit to the pore diameters derived from the cylindrical pore model. The slope of this line gives a pore diameter reduction rate of ~2.3 Å/AB cycle. Assuming the Al_2O_3 is symmetrically deposited on the pore walls, this slope yields an Al_2O_3 growth rate of ~1.2 Å/AB cycle. The dashed line associated with the pore diameters obtained from the aperture pore model yields a Al_2O_3 growth rate of ~1.3 Å/AB cycle. These growth rates were then used to determine the expected change in N_2 conductance versus AB cycles. The solid and dashed lines in Figure 5 display the predicted change in conductance for the cylindrical pore model and aperture pore model, respectively. Figures 5 and 6 show the expected change in the N_2 conductance and pore diameter reduction rate are not strongly dependent on the pore model. The conductance fits displayed in Figure 5 indicate that the aperture model fits the data slightly better.

The observed Al_2O_3 growth rates of 1.2−1.3 Å/AB cycle agree well with previous measurements of 1.1 Å/AB cycle on flat Si (100) substrates.[11] This Al_2O_3 growth rate is larger than the 0.37 Å/AB cycle observed on 200 Å diameter pores in the Anodisc alumina membranes.[8] The surface chemistry of Al_2O_3 growth on the Anodisc alumina membranes was monitored with Fourier transform infrared (FTIR) spectroscopy.[8] The unmodified asymmetric Anodisc membranes consisted of ~2000 Å pores with a ~57 μm thickness and a thin film of ~200 Å pores with a ≤2 μm thickness. Most of the available surface area of the Anodisc membranes and the majority of the FTIR signal were derived from the ~2000 Å pores. The exposure times required for the surface reactions to reach completion were determined from the FTIR spectra. Because of lower conductance in the smaller 200 Å pores, these FTIR measurements may have underestimated the reactant exposures required for complete surface reactions. The lower Al_2O_3 growth rate of 0.37 Å/AB cycle observed on the 200 Å diameter pores in the Anodisc alumina membranes may be attributed, in part, to incomplete surface reactions.

The pore diameters in the porous alumina tubular membranes were reduced from 50 to 5−10 Å with atomic layer control using the sequential surface reactions. A wide range of pore diameters can easily be attained simply by varying the number of AB cycles. No obvious change in the Al_2O_3 growth rate per AB cycle occurs until the pore reduction stops after the 19th AB cycle. Figure 6 shows that the pore diameter reduction is consistent with Al_2O_3 growth rates of 1.2−1.3 Å/AB cycle for pore diameters D < 20 Å. No evidence for a dramatic transition from Knudsen diffusion to configurational diffusion, as described by recent theoretical studies,[23] is observed by the N_2 conductance measurements as the pores reach diameters D < 20 Å in the microporous region.

The pore reduction stops after the 19th AB cycle. No further reduction in pore diameter was observed with further reactant exposures. This behavior may be explained by incomplete surface reactions caused by reduced conductance in the smaller pore diameters. Much longer exposures may be required for a complete reaction after the 19th AB cycle. To test this hypothesis, both TMA and H_2O exposures were increased from 2 to 10 Torr for the 18th−22nd AB cycles. This explanation was ruled out because no Al_2O_3 growth was observed for these increased exposures after multiple reaction cycles.

The stoppage of pore reduction at pore diameters of 5−10 Å after 19 AB cycles may be consistent with the small pore diameters blocking the transport of the TMA and/or H_2O reactants. At the reaction conditions of 2 Torr and 500 K used for TMA deposition, the ratio of the TMA dimer to the TMA monomer is ~0.5:1.[25] The limiting diameter of the TMA dimer is ~5 Å.[26] The TMA monomer has a diameter of ~3 Å. Both the TMA dimer and TMA monomer may be restricted from pore transport after the pore diameter is measured to be 5−10 Å. For comparison, the N_2 molecule used for these conductance measurements has a diameter of ~3.64 Å.[27]

The cessation of pore reduction may also be a result of the different stability of surface species in the molecular-sized pores. Previous studies have shown that the Al_2O_3 deposition rates are directly related to the stability of the OH and CH_3 surface functional groups.[8,11] Past studies have measured a saturation OH coverage of Θ_s ~ 1 OH/10 Å^2 at 300 K.[28,29] Hydroxyl and methyl coverages of $\Theta \sim 0.5\Theta_s$ are stable at the reaction temperature of 500 K on relatively flat Al_2O_3 surfaces.[14] The pores with diameter of 5−10 Å have a surface area of 15−30 Å^2 per 1 Å of pore length. These pores have a predicted OH coverage of ~1 OH per 1 Å of pore length at 500 K. The extreme radius of curvature may affect OH group stability, and even lower coverages may be present on pores with 5−10 Å diameters. The growth rate versus AB cycles may become negligible at these lower coverages.

(25) Carlsson, J.-O.; Gorbatkin, S.; Lubben, D.; Greene, J. E. *J. Vacuum Sci. Technol. B* **1991**, *B9*, 2759.
(26) Greenwood, N. N.; Earnshaw, A. *Chemistry of the Elements*; Pergamon Press: Oxford, 1984.
(27) Chen, N. Y. Deynan, T. F.; Smith, C. M. *Molecular Transport and Reaction in Zeolites: Design and Application of Shape Selective Catalysts*; VCH: New York, 1994.
(28) Peri, J. B. *J. Phys. Chem.* **1965**, *69*, 211.
(29) Hendriksen, B. A.; Pearce, D. R.; Rudham, R. *J. Catal.* **1972**, *24*, 82.

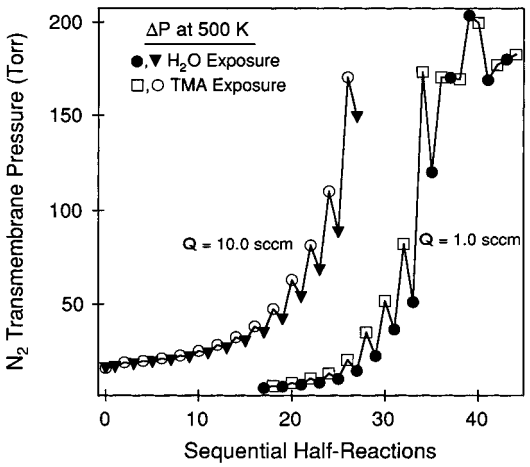

Figure 7. The N_2 transmembrane pressure at 500 K after sequential H_2O (solid symbols) and TMA (open symbols) reactant exposures. These ΔP measurements were performed using two different tubular membranes with N_2 flow rates of $Q = 1.0$ and 10.0 sccm.

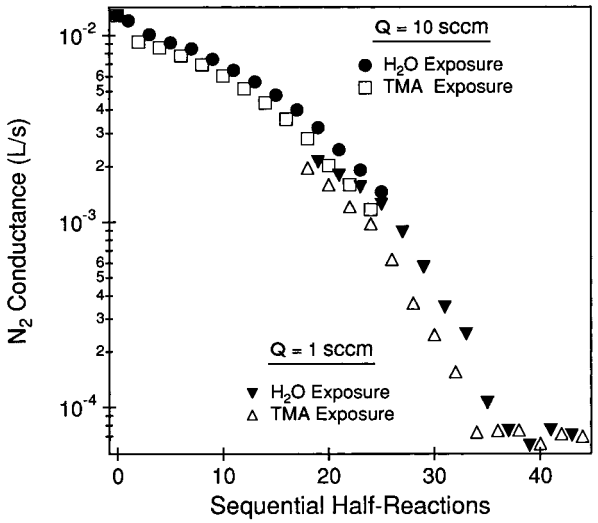

Figure 8. N_2 conductance at 500 K after sequential H_2O (solid symbols) and TMA (open symbols) reactant exposures. These conductances were obtained from transmembrane pressure measurements on two different tubular membranes at N_2 flow rates of $Q = 1.0$ and 10.0 sccm.

Other interpretations may also explain the apparent stoppage of pore reduction at diameters of 5−10 Å. One possible explanation is that there are a small number of relatively large cracks in the tubular membrane or small leaks at the Swagelok seal. The sequential surface chemistry may close all of the pores and leave behind only the small number of cracks or sealing leaks. If the crack diameters or leaks are on the order of ≥1000 Å, these defects would require many more AB cycles to alter their conductance. Consequently, the conductance measured after 19 AB cycles may represent the conductance of the small number of initial cracks in the tubular membrane or sealing leaks. The preliminary gas separations that have been conducted with these modified membranes are consistent with a viscous flow leak through these defects.

Another more speculative interpretation is that the interaction and reactivity of the TMA and H_2O reactant molecules with the pore walls depend on the pore diameter. The separation distance between a weakly bound physisorbed molecule and a surface is ∼2−3 Å. A 3−5 Å diameter TMA monomer or dimer may be pulled equally toward the circumference of pores with a 5−10 Å diameter. This uniform attractive force toward all the pore surfaces could produce a higher adsorption energy and a decreased reactivity caused by "molecular levitation" in the pores.[30,31]

C. Conductance versus Surface Functionality. The N_2 conductance at 500 K was also measured during Al_2O_3 deposition after each H_2O and TMA reactant exposure. The N_2 flow was set with the mass flow controller and the equilibrated transmembrane pressure was recorded after each half-reaction. Figure 7 displays the transmembrane pressure measurements versus the individual H_2O and TMA sequential half-reactions. The solid circles and solid triangles show the ΔP after H_2O exposures that leave OH groups on the pore surface. The open squares and open circles display the ΔP after TMA exposures that leave CH_3 groups on the pore surface. The measurements in Figure 7 were made at N_2 flow rates of $Q = 1$ and 10 sccm for separate alumina membranes.

Figure 7 reveals that the transmembrane pressure is noticeably higher after each TMA exposure. This higher pressure corresponds to a lower membrane conductance after the $AlOH^* + Al(CH_3)_3 \rightarrow AlOAl(CH_3)_2^* + CH_4$ half-reaction that deposits Al and leaves CH_3 groups on the pore surface. In addition, the transmembrane pressure drops significantly after the $AlCH_3^* + H_2O \rightarrow AlOH^* + CH_4$ half-reaction. The lower pressure corresponds to a higher conductance after the H_2O half-reaction that replaces the CH_3 groups with OH groups. Because of the range of the Baratron and complications from the conductance of the gas line, C_g, the $Q = 1$ sccm measurements were most accurate for the smaller pore diameters. The $Q = 10$ sccm measurements were the most accurate for the larger pore diameters.

The corresponding pore conductance was calculated versus the sequential half-reactions using the transmembrane pressure measurements in Figure 7 and eqs 2 and 3. The N_2 conductance measurements for N_2 flow rates of both $Q = 1$ and 10 sccm are shown in Figure 8. Figures 7 and 8 indicate that the transmembrane pressure and pore conductance are strongly dependent on the surface reaction sequence. Figure 8 reveals that the N_2 conductance measured after TMA exposure and deposition of $Al(CH_3)_2$ surface species is significantly smaller than the conductance measured after the previous H_2O exposure. The N_2 conductance measured after the subsequent H_2O exposure that replaces the CH_3 groups with OH groups also consistently displays a larger conductance.

The difference in conductance after the TMA and H_2O exposures reflects the change in the effective pore diameter. Figure 9 shows the calculated pore diameter versus the individual H_2O and TMA reactant exposures assuming Knudsen flow and using the aperture pore model. Very similar results are obtained using the cylindrical pore model. The calculated diameters are

(30) Derycke, I.; Vegeron, J. P.; Lambin, P.; Lucas, A. A.; Derouane, E. G. *J. Chem. Phys.* **1991**, *94*, 4620.
(31) Derouane, E. G.; Andre, J.-M.; Lucas, A. A. *Chem. Phys. Lett.* **1987**, *137*, 336.

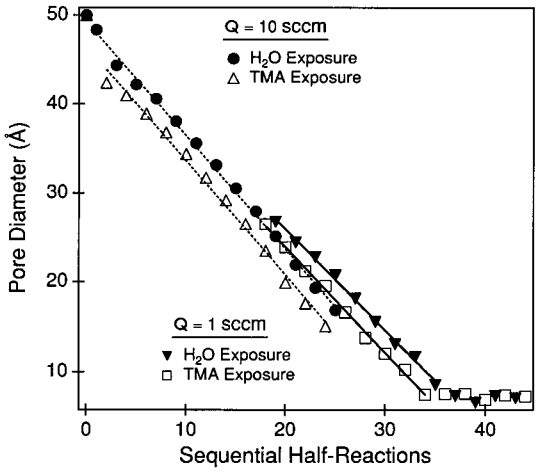

Figure 9. Pore diameters after sequential H_2O (solid symbols) and TMA (open symbols) reactant exposures calculated assuming Knudsen flow and using the aperture pore model. These diameters were derived from N_2 conductance measurements on two different tubular membranes with N_2 flow rates of $Q = 1.0$ and 10.0 sccm.

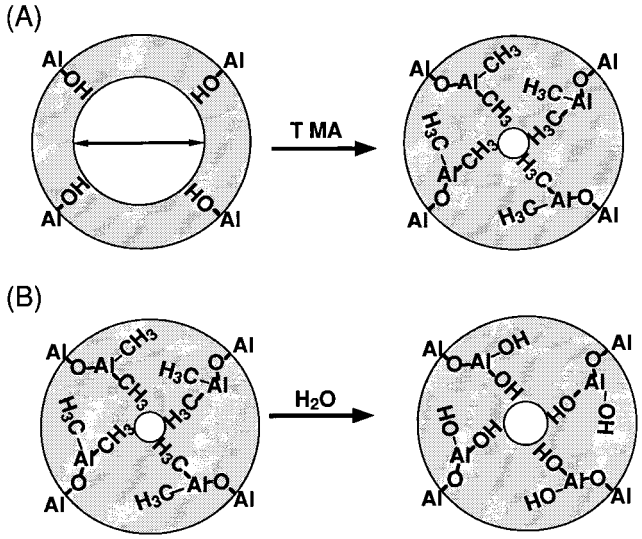

Figure 10. Illustration of the changes in pore diameter during the H_2O and TMA sequential half-reactions.

slightly different for the membranes measured with $Q = 1$ and 10 sccm N_2 flows. The pore diameters obtained from the data at $Q = 10$ sccm predict a diameter that is ~2 Å smaller after 10 AB cycles. This discrepancy can be attributed to minor differences in the initial pore diameters of the two microporous alumina tubular membranes. Slightly varying growth rates may also explain the slight offset between the two data sets.

The measurements at both $Q = 1$ and 10 sccm indicate that the pore diameter measurements are sensitive to the surface functionality. The transmembrane pressures and the corresponding conductances reveal that there is a large decrease in pore diameter after the TMA exposures. This decreased diameter is expected based on the deposition of $Al(CH_3)_2$ species on the pore wall, as illustrated in Figure 10. Figure 9 also shows that the pore diameter increases ~2 Å after the subsequent H_2O exposure. This increase is somewhat surprising because the H_2O exposure should only replace a CH_3 group with an OH group on the surface, as shown in Figure 10.

The increased pore diameter after the H_2O exposure may be attributed to the slightly larger size of a CH_3 group relative to an OH group. The van der Waals diameter of the CH_3 group has been determined to be 3.5−4.0 Å, depending on the definition method.[32,33] Likewise, the van der Waals diameter of the OH group has been determined to be 2.9 Å.[32,33] In agreement with the measurements, these van der Waals diameters predict a larger pore diameter by $\Delta D = 1.2-2.2$ Å after replacing the CH_3 groups with OH groups.

The size of the CH_3 and OH groups on the pore walls can also be approximated from bond length data. The Al−O bond length for an isolated Al−OH group on a single-crystal Al_2O_3 surface has been calculated to be 1.73−1.78 Å.[34] The same calculations found the O−H bond length to be 0.95−1.02 Å. In comparison, bond lengths for Al−C = 1.95 Å[26] and C−H = 1.1 Å[35] are reported for the TMA dimer. These bond lengths indicate that the CH_3 group is only slightly larger than the OH group. Previous ellipsometric measurements during Al_2O_3 deposition also reveal that the film thickness changes only during TMA exposures.[36] These bond length and ellipsometry measurements suggest that only part of the observed $\Delta D \sim 2$ Å is the result of size differences between CH_3 groups and OH groups.

Besides the different van der Waals diameters, the change in conductance after TMA and H_2O exposures may also be caused by different interactions between the N_2 molecule and CH_3 and OH groups on the pore surface. The OH group has a sizable dipole moment of 1.51 D.[32] This dipole may facilitate dipole−induced dipole interactions with the N_2 molecules. This attractive interaction may facilitate additional transport via surface diffusion that would enhance the N_2 conductance. In contrast, CH_3 groups have a somewhat smaller net dipole resulting from a dipole of 0.4 D per C−H bond.[32] This smaller dipole may produce a smaller interaction with N_2 and a smaller surface diffusion contribution.

To test the importance of the interaction between N_2 and the pore surface, argon was used for conductance and pore size measurements at 500 K on a separate alumina tubular membrane. Figure 11 displays the Ar transmembrane pressure versus the individual H_2O and TMA reactant exposures at $Q = 1.39$ sccm. Similar to the N_2 data in Figure 7, the Ar transmembrane pressure at 500 K is sensitive to the sequential surface reactions and the change of surface species. The transmembrane pressure is higher after each $AlOH^* + Al(CH_3)_3 \rightarrow AlOAl(CH_3)_2^* + CH_4$ half-reaction that deposits Al and leaves CH_3 groups on the pore surface. The pressure drops after each $AlCH_3^* + H_2O \rightarrow AlOH^* + CH_4$ half-reaction that replaces CH_3 groups with OH groups. This behavior is very comparable with the results in Figure 7 and also predicts a pore diameter increase of $\Delta D \approx 2$ Å after H_2O exposures.

(32) Israelachvili, J. *Intermolecular and Surface Forces*; Academic Press: San Diego, 1992.
(33) Bondi, A. *Physical Properties of Molecular Crystals, Liquids, and Glasses*; Wiley: New York, 1968.
(34) Blonski, S.; Garofalini, S. H. *J. Phys. Chem.* **1996**, *100*, 2201.
(35) Streitwieser, A.; Heathcock, C. H. *Introduction to Organic Chemistry*; Macmillan: New York, 1985.
(36) Kumagai, H.; Toyoda, K. *Appl. Surf. Sci.* **1994**, *82/83*, 481.

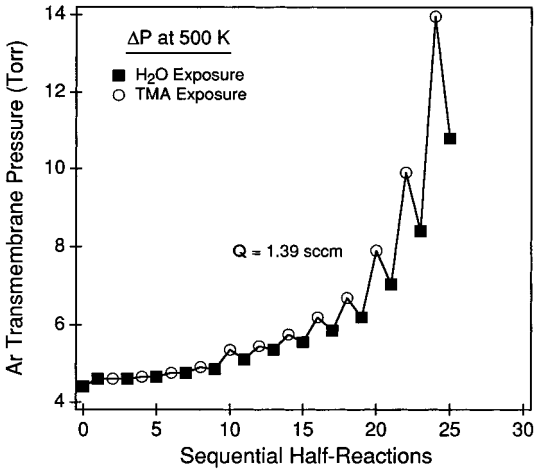

Figure 11. Ar transmembrane pressure at 500 K after sequential H_2O (solid squares) and TMA (open circles) reactant exposures at an Ar flow rate of $Q = 1.39$ sccm.

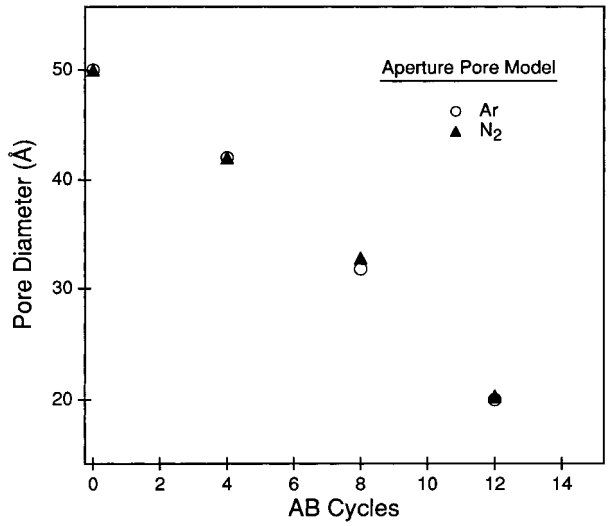

Figure 12. Pore diameters versus AB cycles obtained from Ar (circles) and N_2 (squares) conductance measurements on the same tubular membrane at 298 K assuming Knudsen flow and using the aperature flow model.

To check for possible differences between individual alumina tubular membranes, a series of N_2 and Ar conductance measurements was also performed on the same alumina tubular membrane at 298 K. The pore diameters obtained from these conductance measurements assuming Knudsen flow and using the aperture pore model are shown in Figure 12. Within experimental error, the Ar and N_2 conductance measurements yielded the same pore diameter versus AB cycles. In addition, the ratio of conductances for N_2:Ar was ~1.15 throughout the range of pore diameters. This ratio is in excellent agreement with the expected selectivity from Knudsen diffusion.

Figures 7, 11, and 12 show that the conductance and pore size measurements are unaffected by the measurement gas. This similarity argues that the chemical nature of the interaction between the gas and the surface is not a dominant factor in the conductance measurements. The equivalence between the N_2 and Ar conductance measurements suggests that the pore diameter differences after H_2O and TMA exposures are attributable primarily to the differences between the van der Waals diameters of the OH groups and the CH_3 groups.

However, preliminary investigations of SiO_2 deposition on the mesoporous alumina tubular membranes suggest that gas−surface interactions can be important. A large decrease in N_2 conductance is observed after the first AB cycle during SiO_2 deposition on the porous alumina membrane using $SiCl_4$ and H_2O.[37,38] This decrease in conductance is much larger than expected from a pore diameter reduction of 1−2 Å. The observed decrease may be explained by very different gas−surface interactions on the SiO_2 surface compared with the Al_2O_3 surface. The subsequent conductance decrease versus AB cycles during SiO_2 deposition is consistent with atomic layer controlled growth.

IV. Conclusions

The pore diameters of mesoporous alumina tubular membranes were reduced with atomic layer control using sequential surface reactions. To achieve this atomic layer controlled deposition, the binary reaction $2Al(CH_3)_3 + 3H_2O \rightarrow Al_2O_3 + 6CH_4$ was split into two separate half-reactions. Al_2O_3 was deposited on the mesoporous alumina membranes with atomic layer precision by sequential separate exposures to $Al(CH_3)_3$ (TMA) and H_2O at 500 K. On the basis of earlier investigations of Al_2O_3 growth on flat Si(100) surfaces using TMA and H_2O, each TMA and H_2O reaction cycle at 500 K should deposit ~1.2 Å of Al_2O_3.

The reduction in pore diameter in the alumina membranes after the sequential surface reactions was determined in situ by measuring the transmembrane pressure at a constant N_2 gas flow rate at 298 K. These N_2 pressure measurements yielded the membrane conductance, and the pore diameter could also be determined assuming Knudsen flow using either a cylindrical or aperture pore model. Both models indicated that every TMA and H_2O reaction cycle at 500 K deposited ~1.2 Å of Al_2O_3 on the pore surface. The pore diameters in the alumina membranes were reduced from an initial diameter of ~50 Å to a final diameter of 5−10 Å. No evidence for a transition from Knudsen diffusion to configurational diffusion was observed by the N_2 conducance measurements for pore diameters $D < 20$ Å in the microporous region.

Transmembrane N_2 pressure measurements were also performed at 500 K after each TMA and H_2O exposure. These pressure measurements revealed that the N_2 conductance after the TMA exposure was lower than the conductance after the previous or subsequent H_2O exposure. The TMA reaction leaves CH_3 groups on the pore surface; the H_2O reaction converts the CH_3 groups to OH groups. These conductance measurements indicate that the pore diameters are larger by $\Delta D \sim 2$ Å with OH groups on the pore surface. This difference in pore diameter is close to the difference expected from the van der Waals hard sphere diameters of 3.5−4.0 Å for a CH_3 group and 2.9 Å for an OH group. Additional conductance measurements with Ar displayed the same $\Delta D \sim 2$ Å and confirm that the size of

(37) Klaus, J. W.; Ott, A. W.; Johnson, J. M.; George, S. M. *Appl. Phys. Lett.* **1997**, *70*, 1092.
(38) Sneh, O.; Wise, M. L.; Ott, A. W.; Okada, L. A.; George, S. M. *Surf. Sci.* **1995**, *344*, 135.

surface functional groups can affect gas transport through microporous membranes.

These experiments reveal that the pore diameter in mesoporous membranes can be reduced with atomic layer control using sequential surface reactions. Pore diameters can be progressively reduced to molecular dimensions to tailor microporous membranes for specific gas separation properties. The surface species on the pore surface also play an important role in determining the exact pore diameter. Although the behavior observed in this study may be consistent with the difference in van der Waals hard sphere diameter for CH_3 groups and OH groups, chemical interactions between the gas and surface species may also play an important role.

Acknowledgment. This work was supported by an Exploratory Research Grant from the Chevron Research and Engineering Corp. and the Air Force Office of Scientific Research. We would like to thank Ken McCarley and Prof. Doug Way in the Department of Chemical Engineering and Petroleum Refining at the Colorado School of Mines for providing the mesoporous alumina tubular membranes for this study. We also thank Profs. John Falconer and Rich Noble in the Department of Chemical Engineering at the University of Colorado at Boulder for helpful discussions. The authors also thank Jason Klaus for helpful comments.

CM980384G